ChemPubSoc Europe

DOI: 10.1002/cmdc.201600366

CHEMMEDCHEM Full Papers

Comparison of in Silico, Electrochemical, in Vitro and in Vivo Metabolism of a Homologous Series of (Radio)fluorinated σ_1 Receptor Ligands Designed for Positron Emission Tomography

Christian Wiese,[a] Eva Große Maestrup,[a] Fabian Galla,[a] Dirk Schepmann,[a] Achim Hiller,[b] Steffen Fischer,[b] Friedrich-Alexander Ludwig,[b] Winnie Deuther-Conrad,[b] Cornelius K. Donat,[b] Peter Brust,[b] Lars Büter,[c, d] Uwe Karst,[c, d] and Bernhard Wünsch*[a, d]

The imaging of σ_1 receptors in the brain by fluorinated radiotracers will be used for the validation of σ_1 receptors as drug targets as well as for differential diagnosis of diseases in the central nervous system. The biotransformation of four homologous fluorinated PET tracers 1′-benzyl-3-(ω-fluoromethyl to ω-fluorobutyl)-3*H*-spiro[2]benzofuran-1,4′-piperidine] ([^{18}F]**1**–**4**) was investigated. In silico studies using fast metabolizer (FAME) software, electrochemical oxidations, in vitro studies with rat liver microsomes, and in vivo metabolism studies after application of the PET tracers [^{18}F]**1**–**4** to mice were performed. Combined liquid chromatography and mass spectrometry (HPLC–MS) analysis allowed structural identification of non-radioactive metabolites. Radio-HPLC and radio-TLC provided information about the presence of unchanged parent radiotracers and their radiometabolites. Radiometabolites were not found in the brain after application of [^{18}F]**2**–**4**, but liver, plasma, and urine samples contained several radiometabolites. Less than 2% of the injected dose of [^{18}F]**4** reached the brain, rendering [^{18}F]**4** less appropriate as a PET tracer than [^{18}F]**2** and [^{18}F]**3**. Compounds [^{18}F]**2** and [^{18}F]**3** possess the most promising properties for imaging of σ_1 receptors in the brain. High σ_1 affinity (K_i = 0.59 nM), low lipophilicity (log$D_{7.4}$ = 2.57), high brain penetration (4.6% of injected dose after 30 min), and the absence of radiometabolites in the brain favor the fluoroethyl derivative [^{18}F]**2** slightly over the fluoropropyl derivative [^{18}F]**3** for human use.

Introduction

The σ receptor was first postulated in 1976 by Martin et al., who found that various opioid analgesics exert different pharmacological profiles.[1] This observation led to the sub-differentiation of the opioid receptor into three opioid receptor subtypes, which were termed according to their prototypical ligands μ (morphine), κ (ketocyclazocine), and σ receptors (SKF-10,047).[1,2] Because typical opioid antagonists such as naloxone and naltrexone are unable to inhibit the effects caused by σ ligands, the σ receptor was removed from the class of opioid receptors.[3] Today σ receptors represent a unique class of non-opioid, non-NMDA, and non-dopamine receptors, which are classified into σ_1 and σ_2 receptor subtypes.[4,5] Herein we focus on the σ_1 receptor subtype.

Cloning of the σ_1 receptor led to a protein with 223 amino acids and a molecular weight of 25.3 kDa, which is not related to any other mammalian protein. It shares a 30% homology with the yeast enzyme sterol-Δ^8/Δ^7-isomerase.[6,7] The σ_1 receptor is composed of two transmembrane helices, an extracellular loop (50 residues), a short N-terminal domain (10 residues) and a long C-terminal domain containing the ligand binding site. Both the N- and C-terminal domains are located intracellularly.[8] Very recently a 3D homology model of the σ_1 receptor was reported showing the 3D organization of the protein and its interaction with ligands. A combined site-directed mutagenesis and theoretical analysis of the receptor protein provided profound insight into the receptor–ligand interactions at the molecular level.[9,10]

The σ_1 receptor is located within the membrane of the endoplasmic reticulum, but also within the cell membrane and the membrane of mitochondria. It controls the Ca^{2+} transfer from the endoplasmic reticulum to mitochondria via interaction with the Ca^{2+} binding chaperone BiP (binding immunoglobulin protein) and the inositol triphosphate receptor.[11–13]

[a] Dr. C. Wiese, Dr. E. Große Maestrup, Dr. F. Galla, Dr. D. Schepmann, Prof. Dr. B. Wünsch
Institut für Pharmazeutische und Medizinische Chemie, Westfälische Wilhelms-Universität Münster, Corrensstraße 48, 48149 Münster (Germany)
E-mail: wuensch@uni-muenster.de

[b] Dr. A. Hiller, Dr. S. Fischer, Dr. F.-A. Ludwig, Dr. W. Deuther-Conrad, Dr. C. K. Donat, Prof. Dr. P. Brust
Helmholtz-Zentrum Dresden-Rossendorf, Institut für Radiopharmazeutische Krebsforschung, Forschungsstelle Leipzig, Permoserstraße 15, 04318 Leipzig (Germany)

[c] Dr. L. Büter, Prof. Dr. U. Karst
Institut für Anorganische und Analytische Chemie, Westfälische Wilhelms-Universität Münster, Corrensstraße 30, 48149 Münster (Germany)

[d] Dr. L. Büter, Prof. Dr. U. Karst, Prof. Dr. B. Wünsch
Cells-in-Motion Cluster of Excellence (EXC 100–CiM), Westfälische Wilhelms-Universität Münster, 48149 Münster (Germany)

Supporting information for this article can be found under http://dx.doi.org/10.1002/cmdc.201600366.

© 2016 Wiley-VCH Verlag GmbH & Co. KGaA, Weinheim

These are not the final page numbers! ↗↗

Moreover, it has been shown that σ_1 receptors are able to regulate K^+ and Na^+ channels.[14,15] In addition to the influence on ion channels, σ_1 receptors modulate various neurotransmitter systems including the cholinergic, dopaminergic and glutamatergic neurotransmission.[16–18]

A high density of σ_1 receptors is not only found in the central nervous system (CNS), but also in various tissues of the periphery, including heart, kidney, liver, endocrine organs, and placenta. In the CNS, a high density of σ_1 receptors is found in the frontal cortex, hypothalamus, hippocampus, and cerebellum regions associated with memory and emotion as well as motor and sensory control.[19–22]

It has been shown that the σ_1 receptor is involved in several psychiatric and neurodegenerative disorders including depression, psychosis, anxiety, neuropathic pain and Alzheimer's and Parkinson's disease.[22–25] The naphthyl substituted pyrazole derivative S1RA is currently being investigated in phase II clinical trials of neuropathic pain.[26–28] Due to the important role of the σ_1 receptor in the above mentioned psychiatric and neurodegenerative disorders, imaging of the σ_1 receptor in positron emission tomography (PET) studies is of particular interest. A PET tracer suitable for imaging of σ_1 receptors in the brain will be used for target validation with the aim of developing novel therapeutic concepts. Moreover, a correlation of σ_1 receptor density and activity with a particular disease could be exploited for diagnosis and prognosis.[29]

Recently, a set of four homologous fluoroalkyl-substituted spirocyclic σ_1 receptor ligands **1**–**4** has been synthesized and pharmacologically evaluated (Figure 1). Due to the high σ_1 receptor affinity (K_i = 0.59–1.4 nM) and selectivity against the σ_2 subtype and other related receptors, the compounds **1**–**4** were labeled with [^{18}F]fluoride and investigated as PET tracers for imaging of σ_1 receptors in the brain. With respect to organ distribution and pharmacokinetic properties the fluoroethyl derivative **2** (fluspidine) represents the most promising radioligand and is currently used in clinical studies.[30–38]

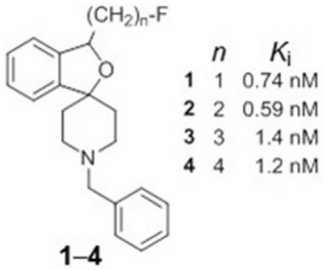

Figure 1. Homologous fluorinated spirocyclic σ_1 receptor ligands **1**–**4** developed for imaging of σ_1 receptors in the brain.

For studies with living organisms the biotransformation of the respective ligand has to be considered. During the development of a PET tracer the metabolism is of particular interest, since the tracer should have a biological half-life longer than the period of observation, usually at least 30–60 min. In general, aliphatic C–F bonds are rather stable. Nevertheless, primary alkyl fluorides can be defluorinated by elimination, substitution or oxidation losing the [^{18}F]label. Moreover, radioactive metabolites penetrating the blood–brain barrier (BBB) will lead to distorted images.

In this manuscript the biotransformation of the homologous fluorinated σ_1 receptor ligands **1**–**4** is reported. After prediction of metabolically labile positions using the software package Fast Metabolizer (FAME), the products formed by electrochemical oxidation were analyzed. Then, the in vitro metabolism during incubation with rat liver microsomes was investigated and the formed metabolites were compared with the predicted and electrochemically formed metabolites. Finally, the radiometabolites formed after injection of the [^{18}F]-labeled tracers [^{18}F]**1**–[^{18}F]**4** in mice were characterized.

Results and Discussion

Prediction of metabolically labile positions by FAME

Data about phase 1 and phase 2 metabolites of a large number of organic molecules are collected in FAME.[39] Based on this information, heavy atoms of unknown compounds are ranked according to the probability of being involved in a biotransformation reaction. Values between 0 and 1 are attributed to the heavy atoms; a value of 0 indicates a low and a value of 1 a high probability of the heavy atom being involved in a biotransformation reaction. In this study, heavy atoms showing a value greater than 0.22 were considered. In Figure 2 the heavy atoms of **1**–**4** predicted by FAME as potentially metabolically labile positions are marked with arrows.

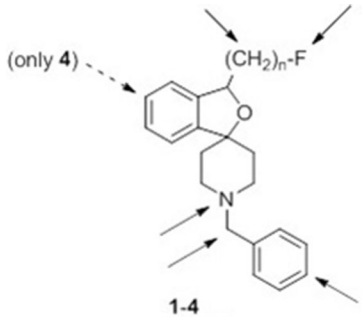

Figure 2. Metabolically labile positions predicted by FAME using the algorithm for rat phase 1 reactions; black arrows indicate metabolically labile positions; the dashed arrow indicates a position which was only predicted for the phenylbutyl derivative **4**.

According to the predictions of FAME the N atom and the adjacent benzylic C atom have the highest probability for metabolic reactions. Additionally, the *para* position of the benzyl moiety was identified as metabolically labile. For all homologs, C atoms of the side chain and the terminal fluorine atom were marked as metabolically labile positions. Unexpectedly, the benzene ring of the benzofuran was predicted only for the fluorobutyl derivative **4**. Here, the C atom at position 5 was predicted to be biotransformed.

© 2016 Wiley-VCH Verlag GmbH & Co. KGaA, Weinheim

Electrochemical oxidation of 1–4

The CYP-catalyzed oxidative biotransformation of compounds **1**–**4** can also be simulated by means of electrochemical oxidation. Subsequent mass spectrometric detection and the absence of biological matrices allow the identification of reactive and short-lived species such as radical cations as well as to evaluate their binding tendency toward selected biomolecules.[40–44] To investigate the oxidative biotransformation of compounds **1**–**4** electrochemically, a potential ramp was applied to the electrochemical cell and the detected mass spectra were plotted depending on the applied oxidation potential. The obtained mass voltammograms allow an easy identification of possible biotransformation products, since electrochemically generated oxidation products typically show increasing signal intensities during the potential ramp, while the signal intensity of the starting compound is decreasing.

In Figure 3, the mass voltammogram of **1** is shown. The signal intensity of **1** (*m/z* 312) starts to decrease at a potential of ~1.7 V. At the same time, several signals appear with increasing intensities. The signal of *m/z* 328, which can be traced back to a hydroxylated oxidation product of **1**, is already present without applying a potential. This can be explained by the fact that electrochemical oxidations can also occur during the electrospray ionization process. However, this is the only oxidation product present in the mass spectrum of the initial solution. Based on the detected exact masses of all indicated oxidation products, sum formulae were determined and chemical structures were deduced.

In Figure 4, the suggested structures of the oxidation products of compounds **1**–**4** are shown. Hydroxylation of the benzofuran moiety (e.g., **1g**–**4g**), dehydrogenation of the piperidine ring (e.g., **1k**–**4k**), N-debenzylation (e.g., **1a**–**4a**), and all possible combinations of these reactions (e.g., **1h**–**4h**, **1i**–**4i**, **1m**–**4m**) have taken place. The position of the hydroxy group cannot be specified based on the exact masses, but the presence of oxidation products resulting from N-debenzylation and hydroxylation indicates that hydroxylation probably has taken place at the positions labeled in the respective structures shown in Figure 4. For the homologous fluoroalkyl derivatives **1**–**4**, very similar oxidation products were detected. However, in the case of the fluoroethyl derivative **2**, the hydroxylated and N-debenzylated product **2i** was not detected, indicating that further dehydrogenation of **2i** to form **2j** or dehydrogenation of the corresponding precursors **2a** and **2g** have already taken place quantitatively.

A comparison of in silico predicted (FAME) and electrochemically generated metabolites shows that the N atom and the adjacent benzylic C atom are the most labile positions. In contrast to the in silico prediction, electrochemical oxidation of the fluoroalkyl side chain was not detected. However, the benzene ring of all four homologs was oxidized electrochemically, although this biotransformation reaction was predicted only for the fluorobutyl derivative **4**.

In vitro metabolism using rat liver microsomes

Analysis of metabolites formed upon incubation of 1–4 with rat liver microsomes and NADPH

To analyze the metabolic labile positions, the fluoroalkyl-substituted σ_1 ligands **1**–**4** were incubated with rat liver microsomes and Nicotinamide adenine dinucleotide phosphate (NADPH). After precipitation of the proteins with acetonitrile, the supernatant containing the metabolites was analyzed by HPLC–HRMS methods.

In general six metabolites of the homologous fluoroalkyl-substituted derivatives **1**–**4** could be identified (Figure 5). The secondary amines **1a**–**4a** belong to the main metabolites. Their exact mass indicates the removal of the N-benzyl group by cytochrome P450 (CYP) catalyzed dealkylation. Moreover, the structures of the fluoroethyl and fluoropropyl derivatives

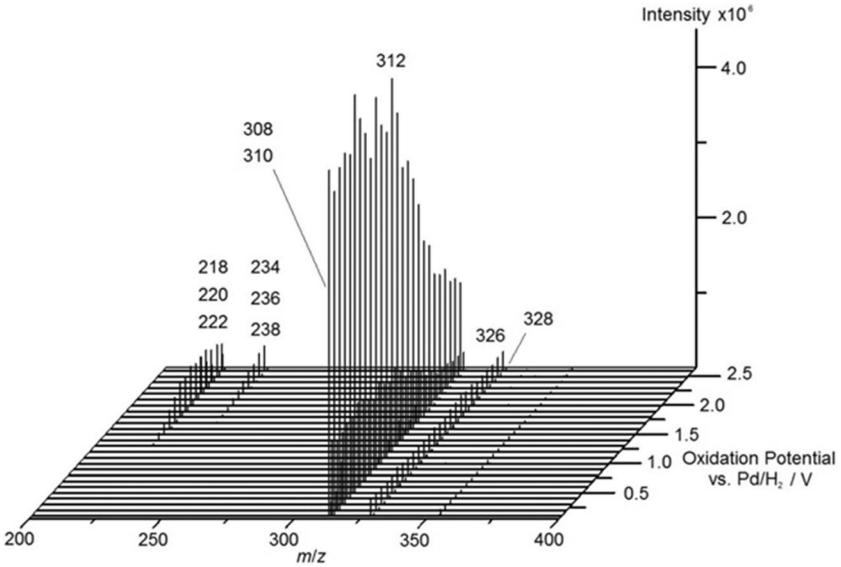

Figure 3. Mass voltammogram obtained from the electrochemical oxidation of compound **1**. The signal intensity of **1** (*m/z* 312) is decreasing, while signals for oxidation products appear with increasing signal intensities. For clarity only normal mass values of oxidation products are shown.

© 2016 Wiley-VCH Verlag GmbH & Co. KGaA, Weinheim

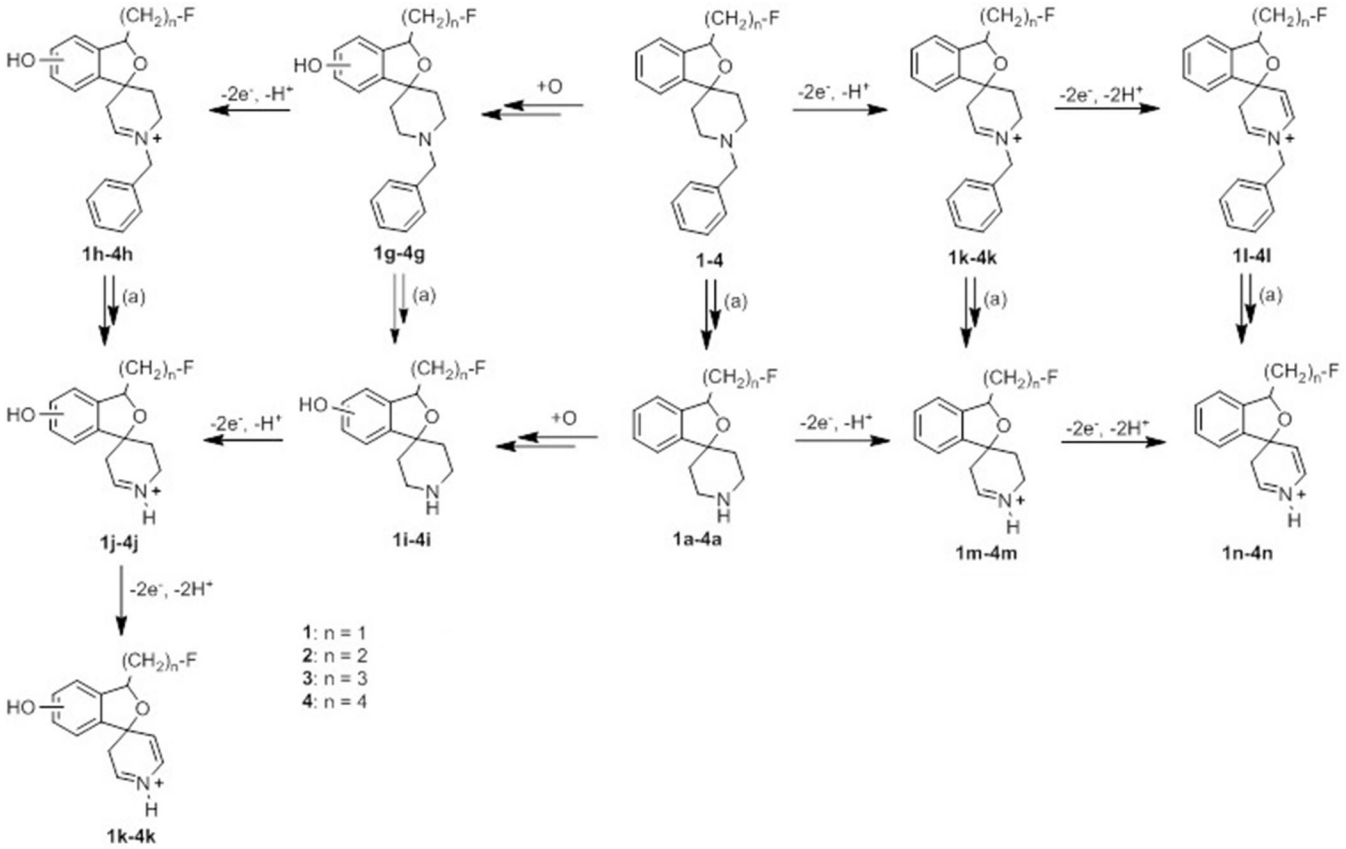

Figure 4. Possible oxidation pathway of compounds **1**–**4**. Structural formulae were deduced based on the determined sum formulae, which were obtained from the detected exact masses. (a) Electrochemical N-debenzylation.

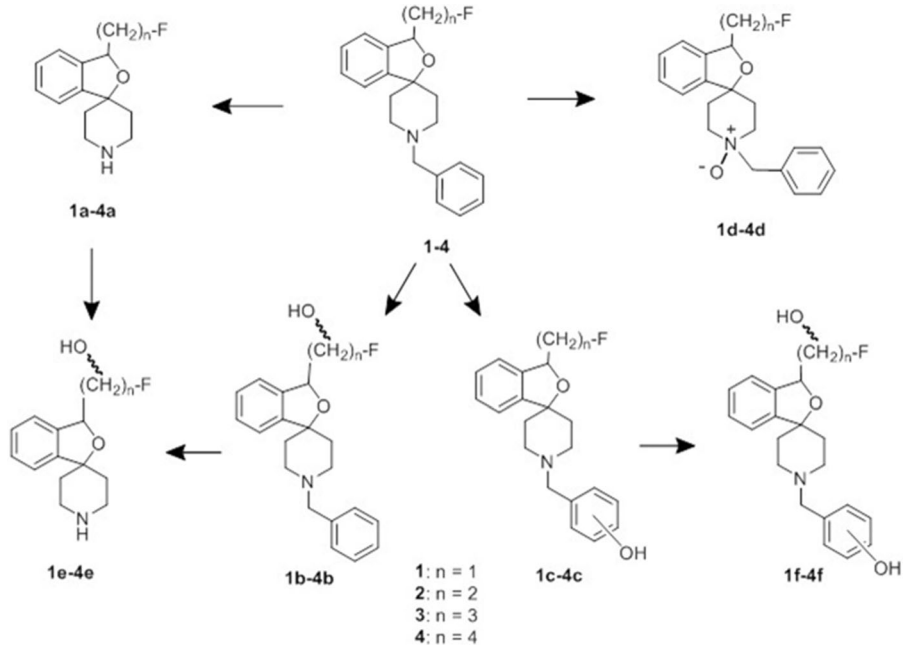

Figure 5. Metabolites formed by incubation of **1**–**4** with rat liver microsomes and NADPH. Metabolites of **2** and **3** have already been reported.[33,36]

2a and **3a** were confirmed unequivocally by comparison of the retention times and mass spectra with independently synthesized compounds.[32,36]

Three monooxygenated products were formed by CYP catalyzed oxidation, respectively. Compounds **1b**,**c**–**4b**,**c** bearing the additional oxygen atom in the fluoroalkyl side chain or the

© 2016 Wiley-VCH Verlag GmbH & Co. KGaA, Weinheim

benzyl moiety represent important metabolites. In the MS analyses of the hydroxybenzyl metabolites **1c–4c** fragments with a mass decreased by 106 Da were detected. It is assumed that the $M+H^+-106$ fragment results from the cleavage of the hydroxybenzyl moiety. Additionally, the fragments $M+H^+-106$ of the metabolites **1c–4c** are identical with the fragments $M+H^+-91$ of the parent compounds **1–4** and produce the same fragmentation pattern. The 4-hydroxybenzyl substituted compound **2c** had been synthesized to prove the structure of this metabolite and furthermore the position of the OH moiety in the *para* position.[34]

The fragmentation pattern of the metabolites **1b–4b** excludes hydroxylation in the benzyl moiety and the piperidine ring. The stepwise fragmentation of the metabolite **2b** showed elimination of the benzyl moiety ($M+H^+-91$) and subsequent loss of two molecules of water ($M+H^+-91-18$ and $M+H^+-91-18-18$). The removal of two molecules of water is only possible if the OH moiety is in an aliphatic position, that is, in the fluoroalkyl side chain. The first H_2O molecule resulted from removal of the additional hydroxy moiety, the second one stems from the benzofuran subunit. Moreover, in the chromatogram, the metabolite **2b** shows two peaks close together with the same exact mass and the same fragmentation pattern. These peaks could result from two diastereomeric metabolites, since hydroxylation in the fluoroalkyl side chain led to an additional center of chirality.

The retention times during RP-HPLC of the third monooxygenated metabolites **1d–4d** were longer than those of the parent compounds **1–4** indicating higher lipophilicity of the metabolites. This observation together with the fragmentation pattern points to the corresponding N-oxides **1d–4d**. The N-oxides **2d** and **3d** derived from the fluoroethyl and fluoropropyl derivatives **2** and **3** had been prepared independently confirming the structures **1d–4d**.[34,37]

The secondary amines **1e–4e** with a hydroxy moiety in the fluoroalkyl side chain represent the most polar metabolites. After elimination of water (aliphatic OH group) in MS^n fragmentation experiments, the further fragmentation patterns were very similar to the fragmentation patterns of the metabolites **1a–4a**. Additionally, the twin peaks in the chromatogram indicate the existence of diastereomers originating from the additional OH group in the fluoroalkyl side chain.

In addition to monooxygenated metabolites **1b,c,d–4b,c,d**, incubation with rat liver microsomes produced one dihydroxylated metabolite **1f–4f**, respectively. The mass of the main fragment after cleavage of the hydroxybenzyl moiety ($M+H^+-106$) was identical to the mass of the metabolites **1e–4e**. Moreover, the fragmentation pattern of the main fragments and the metabolites **1e–4e** were very similar pointing to the metabolites **1f–4f** bearing an N-(hydroxybenzyl) moiety and an additional OH moiety in the fluoroalkyl side chain. This comparative study leads to the conclusion that incubation of the four homologous fluoroalkyl substituted spirocyclic σ_1 ligands **1–4** with rat liver microsomes produced very similar patterns of metabolites.

As predicted by FAME, the secondary amines **1a–4a** formed by oxidative debenzylation represent the main metabolites of the four homologous fluoroalkyl derivatives **1–4** after incubation with rat liver microsomes and electrochemical oxidation. In addition to N-debenzylation, rat liver microsomes oxidized compounds **1–4** at the fluoroalkyl side chain (**1b–4b**), the benzyl moiety (**1c–4c**), and the N atom (**1d–4d**). These positions were also predicted by FAME. In contrast, the electrochemical oxidation did not modify the fluoroalkyl side chain and the phenyl ring of the benzyl moiety. Nevertheless, dehydrogenation of the piperidine ring (**1k–4k**) was observed during electrochemical oxidation, which could be the first step in oxidative transformations around the tertiary amine. The predicted and detected (electrochemical oxidation) products with a hydroxy moiety in the benzofuran ring (**1g–4g**) could not be found after incubation with rat liver microsomes.

Kinetics of metabolic degradation

Next, the stability of the four homologous fluoroalkyl substituted spirocyclic σ_1 ligands **1–4** during incubation with rat liver microsomes and NADPH was determined. For this purpose, incubations were stopped after 5, 10, 30, 40, 60 and 90 min, by addition of cold (−20 °C) acetonitrile. The amount of remaining parent compound **1–4** was determined by HPLC. A matrix matched calibration was performed without addition of NADPH using the compound concentration in the assay as highest calibration concentration.

The metabolic degradation of the ligands **1–4** is shown in Figure 6. It can be seen that the fluoropropyl and fluorobutyl derivatives **3** and **4** with the elongated side chains are more stable than the corresponding fluoroethyl and fluoromethyl derivatives **2** and **1** with shorter side chains. After an incubation period of 90 min, ~25–30% of the parent compounds **3** and **4** were still detected, but 90% of **1** and almost 100% of **2** were metabolized by the microsome preparation.

The amount of unchanged parent compound after an incubation period of 30 min is of particular interest, since PET studies are usually performed during this period of time. The fluoropropyl derivative **3** represents the most stable compound of this series of fluorinated ligands with 46% of the parent com-

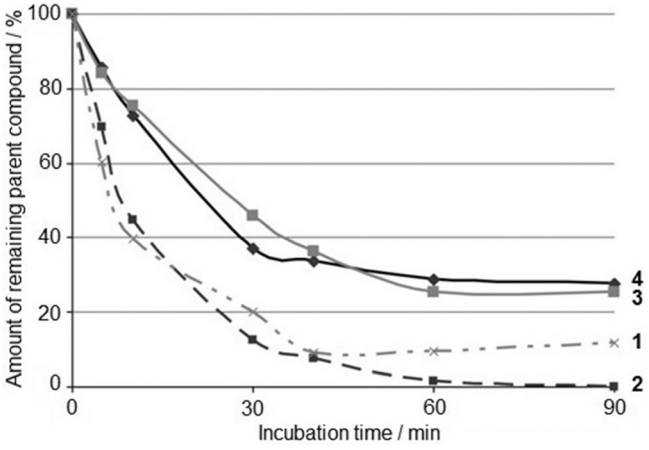

Figure 6. Degradation of the four homologous fluoroalkyl derivatives **1–4** over time during incubation with rat liver microsomes and NADPH.

© 2016 Wiley-VCH Verlag GmbH & Co. KGaA, Weinheim

pound remaining unchanged after 30 min. The longer fluorobutyl derivative **4** showed almost the same stability (36% unchanged after 30 min). However, the metabolic stability of the fluoromethyl and fluoroethyl derivatives **1** and **2** was considerably lower than the stability of **3** and **4**, since only 20% and 13% of the parent compounds remained unchanged after an incubation period of 30 min.

It can be concluded that the fluoropropyl derivative **3** is metabolically the most stable and the fluoroethyl derivative **2** is metabolically the least stable ligand of this series of fluorinated compounds. However, these results have to be interpreted very carefully, since the rate of degradation in vivo depends also on parameters such as lipophilicity, plasma protein binding, penetration into the tissue, etc. In order to image σ_1 receptors in the brain the penetration of the ligands into the brain and the absence of radiometabolites in the brain are important features.

In vivo metabolism of [^{18}F]1–[^{18}F]4 in mice during PET studies

Radiosynthesis

The fluorinated PET tracers [^{18}F]**1**–[^{18}F]**4** were synthesized as previously described.[30,33,36,38] In brief the tosylates **5**–**8** were reacted with [^{18}F]fluoride in the presence of the cryptand Kryptofix K2.2.2 (Figure 7). Heating of the acetonitrile solutions of **6**–**8** for 15 min provided the fluorinated PET tracers [^{18}F]**2**–[^{18}F]**4** in reproducible high labeling yields of ~55–70%. However, the synthesis of the fluoromethyl derivative [^{18}F]**1** required heating of the components in DMSO (150 °C). The sterically demanding 2-benzofuran system close to the reaction center is the reason for the sluggish reaction of the tosylate **5**. In general radiochemical yields of 35–40%, radiochemical purity of $\geq$99%, high chemical purity (free from non-radioactive compounds) and a specific activity of $\geq$200 GBq μmol^{-1} within a total synthesis time of 90–120 min were obtained for all radiotracers.

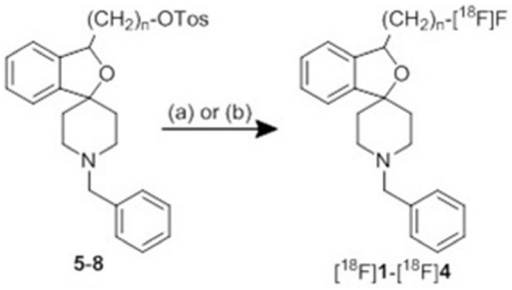

Figure 7. Radiosynthesis of [^{18}F]**1**–[^{18}F]**4**: (a) K[^{18}F]F, K2.2.2, DMSO, 150 °C, 25 min, for [^{18}F]**1**; (b) CH_3CN, 85 °C, 15 min for [^{18}F]**2**–[^{18}F]**4**.

Recovery of PET tracer [^{18}F]2 from complex biological matrices

To analyze the metabolites formed in vivo after application of the fluorinated tracers [^{18}F]**1**–[^{18}F]**4** to mice, the recovery of the parent compounds from biological matrices was investigated. In the majority of radiometabolite experiments, brain and liver homogenates (tissues) as well as blood plasma and urine (biofluids) were analyzed. Investigation of radiometabolites in the brain is of major interest, since it represents the target organ of the tracer. Analysis of plasma samples is also crucial for studying metabolic pathways and for modelling of PET data. The liver is the central organ responsible for the biotransformation of exogenous compounds. Polar metabolites are preferentially excreted via the kidney and urine and, therefore, the radiometabolites in the urine were determined.

The first essential step in studying radiometabolites in tissues and biofluids is the separation of low molecular weight analytes from the biological matrix components in particular macromolecular components such as proteins. Generally more than 85% of the activity of the parent radiotracer and its metabolites should be extracted. Due to the complexity of matrix components, radiotracers and radiometabolites as well as their interactions, a general method for separation does not exist. However, protein precipitation is the most commonly used method.[45,46]

Despite their strong precipitation efficiency, strong acids such as $HClO_4$, and trichloroacetic acid are not suitable, since they are chemically too aggressive and can lead to decomposition of acid labile metabolites. Organic solvents (CH_3CN, CH_3OH, EtOH, acetone) and solvent mixtures (CH_3CN/CH_3OH, CH_3OH/CH_2Cl_2, CH_3OH/EtOH, CH_3CN/H_2O, CH_3OH/CH_3CN/acetone) are preferred precipitation agents.

To investigate the recovery of fluorinated PET tracers from complex biological matrices, [^{18}F]**2** (fluspidine) was selected as model compound. A defined amount of [^{18}F]**2** was added to freshly prepared biomaterials obtained from different sources and various extracting agents were used. Plasma (rabbit), brain homogenates (mouse) and liver homogenates (pig) were employed as biomaterials and CH_3CN (100%, 90% and 80%) as well as CH_3OH (100%, 90% and 80%) were used for the precipitation of proteins and further matrix components. The first precipitation step already provided $\geq$90% of the total ^{18}F activity in the supernatant (radio-HPLC). A second extraction step increased the extracted activity less than 5% indicating that the first extracting step was already very efficient.

Extraction of brain, plasma and liver samples with different precipitation media resulted in very high amounts of the intact parent radiotracer [^{18}F]**2** (96–99%) as monitored by radio-TLC. These results indicate very low protein binding of the PET tracer and negligible matrix effects. However, the UV signals (254 nm) of the HPLC chromatograms of samples prepared using different extraction media showed significant differences. Whereas CH_3OH as well as aqueous CH_3OH and CH_3CN revealed some UV-active impurities, samples extracted with pure CH_3CN provided very clean chromatograms. Therefore, CH_3CN was chosen as the preferred precipitating agent in further experiments.

Additionally to these experiments, bovine serum albumin was incubated with [^{18}F]**2** and subsequently the sample was precipitated with cold CH_3CN. The recovery of the PET tracer was >98%. According to the method of Bradford residual pro-

© 2016 Wiley-VCH Verlag GmbH & Co. KGaA, Weinheim

tein components were not found in the extract indicating complete precipitation of the proteins. The ratio of biomaterial and precipitating agent was crucial. Whereas a ratio of biomaterial: precipitating agent of 1:2 was somewhat critical to give a good pellet, a ratio of 1:3 or 1:4 led to formation of good pellets.

In summary, cold CH_3CN used in three- to four-fold excess over the biomaterial represents the preferred procedure to extract the fluorinated PET tracers [^{18}F]**1**–[^{18}F]**4** and their metabolites almost quantitatively from the biomaterial.

Analysis of radiometabolites of [^{18}F]1–[^{18}F]4 in different tissues and biofluids

To analyze radiometabolites in different tissues and biofluids, brain and liver samples were homogenized and urine and plasma samples were used directly. The proteins of the samples were precipitated by cold CH_3CN.

Radiometabolites of [^{18}F]1–4 found in mouse brain

In brain, more than 95% of intact radiotracers [^{18}F]**2**–**4** were present at 30 min and 60 min after injection (Table 1). At these time points, radiometabolites could not be detected indicating that radiometabolites were not formed in the brain and radiometabolites potentially formed in the periphery could not pass the BBB.

Table 1. Amount of parent compounds [^{18}F]**1**–**4** and recovery in mouse brain samples 30 and 60 min after injection (extraction agent: CH_3CN).

Compd	30 min[a]		60 min[a]	
	intact radiotracer [%][b]	recovery [%][c]	intact radiotracer [%][b]	recovery [%][c]
[^{18}F]**1**	91 ± 2.5	75–80	81 ± 2.0	60–68
[^{18}F]**2**	97 ± 1.1	50–60	98 ± 0.5	65–70
[^{18}F]**3**	96 ± 1.5	85–90	98 ± 1.4	80–85
[^{18}F]**4**	96 ± 1.0	80–85	95 ± 2.7	85–95

[a] Time after radiotracer injection. [b] Mean values ± SD ($n = 3$) from radio-TLC and radio-HPLC experiments. [c] Amount of activity in the CH_3CN extract relative to the total activity in the respective brain sample.

Notably, the fluoromethyl compound [^{18}F]**1** differed significantly from [^{18}F]**2**–**4** (Table 1, and Supporting Information (SI) Figure SI1). HPLC analysis resulted in two radioactive compounds at shorter retention times of 35 min (compound **1-A**) and 26 min (compound **1-B**) indicating higher polarity of these radiometabolites than the parent compound [^{18}F]**1**. The amount of both radiometabolites increased over the time. At 30 min after injection of [^{18}F]**1**, the amount of radiometabolites was 6% (**1-A**) and 4% (**1-B**), whereas at 60 min, 9% and 12% of the radiometabolites **1-A** and **1-B** were found, respectively (Figure SI1). In parallel, the amount of intact radiotracer [^{18}F]**1** decreased from 90% (30 min) to 79% (60 min). HPLC and TLC data were in agreement (±3%). The reproducibility of the results was excellent, considering the natural variability of animal experiments. The recovery was lower than expected (60–90%). As the amount of intact radiotracer was always >90% (exception [^{18}F]F**1** after 60 min), it is difficult to determine whether the extraction of the parent compounds or their radiometabolites is incomplete.

The relative activity in mouse brain at 30 min and at 60 min after injection derived from organ distribution studies of [^{18}F]**1**–**4** is depicted in Figure 8. The relative amount of the metabolically more stable radiotracers [^{18}F]**2**–**4** decreased in the order [^{18}F]**2** > [^{18}F]**3** > [^{18}F]**4**. The log*D* values at pH 7.4 increase in the same order indicating that the uptake of the intact radiotracer decreases with increasing lipophilicity. It is assumed that the more lipophilic fluorobutyl derivative [^{18}F]**4** is trapped partly within membranes.[38]

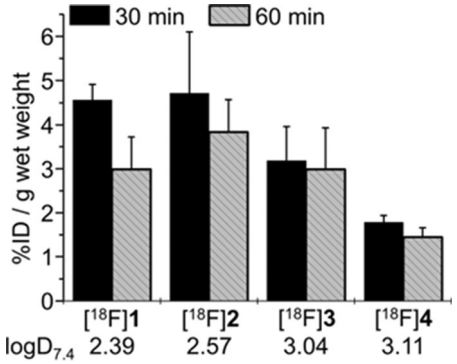

Figure 8. Relative amounts of activity in mouse brain 30 min and 60 min after injection of radiotracers [^{18}F]**1**–**4**. Doses were standardized related to wet weight; data are mean values ± standard deviation; number of experiments $n = 3$–5; distribution coefficients at pH 7.4 ($\log D_{7.4}$) were recorded by distribution of the radiotracers between *n*-octanol and phosphate buffer pH 7.4 and subsequent quantification of activity.[30,33,36,38]

A similar trend was reported for N-([^{18}F]fluoroalkyl)spiperone derivatives, where increasing lipophilicity led to decreased amounts of radiotracers in the brain. However, the $\log D_{7.4}$ values of fluorinated spiperone derivatives are higher than the $\log D_{7.4}$ values of the radiotracers [^{18}F]**1**–**4** and differ more from each other. Within this series of fluoroalkyl spiperone derivatives the preference was given to metabolically more stable compounds.[47]

The absence of radiometabolites in the brain together with the high relative amount of radiotracer in the target tissue brain (4.6% of injected dose) render the fluoroethyl derivative [^{18}F]**2** the favored radiotracer of this series of homologs.

Radiometabolites of [^{18}F]1–4 found in mouse liver

Because the liver plays a central role in the biotransformation of xenobiotics and their excretion, the presence of radiotracers [^{18}F]**1**–**4** and their radiometabolites in mouse liver homogenates was analyzed; 30 min after injection, the amounts of unchanged radiotracers [^{18}F]**2**–**4** in the liver sample were rather similar (57–69%), but the amount of intact fluoromethyl derivative [^{18}F]**1** was only 27% (Table SI1). Clearly, the biotransformation of the fluoromethyl derivative [^{18}F]**1** is faster than the

© 2016 Wiley-VCH Verlag GmbH & Co. KGaA, Weinheim

biotransformation of the longer chained homologs [^{18}F]**2**–**4**. Surprisingly, the amounts of [^{18}F]**1**, [^{18}F]**3** and [^{18}F]**4** remained constant between 30 and 60 min after injection, whereas the fluoroethyl derivative [^{18}F]**2** was further biotransformed.

All detected radiometabolites were more polar than the corresponding parent compounds [^{18}F]**1**–**4**. However, neither in radio-TLC nor in radio-HPLC was a signal for [^{18}F]fluoride observed. At 30 min after injection, radio-HPLC of liver samples showed three major metabolites **1-A**, **1-B** and **1-D** for the fluoromethyl derivative [^{18}F]**1**. At the same time, the chromatograms of liver samples of mice treated with the homologous fluoroalkyl derivatives [^{18}F]**2**–**4** were very similar considering the increasing retention times of homologs with longer alkyl chains (Figure 9). The corresponding radio-HPLC chromatograms of liver samples at 60 min after injection of the radiotracers [^{18}F]**1**-**4** were very similar to the chromatograms obtained at 30 min.

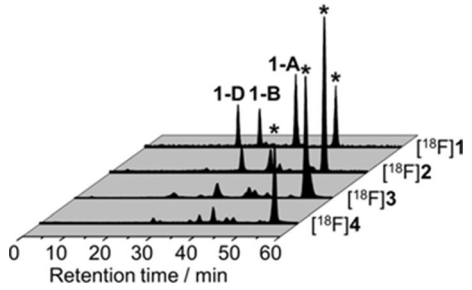

Figure 9. Chromatograms of radioactive metabolites of tracers [^{18}F]**1**–**4** detected by radio-HPLC in samples of mouse liver at 30 min after injection (extraction agent CH_3CN). Retention times of parent compounds: [^{18}F]**1**: t_R = 44.5 min; [^{18}F]**2**: t_R = 49.9 min; [^{18}F]**3**: t_R = 53.7 min; [^{18}F]**4**: t_R = 54.7 min.

In Figure SI2 the chromatograms of liver samples at 30 min after injection of the fluoromethyl and fluoroethyl radiotracers [^{18}F]**1** and [^{18}F]**2** are compared. For the fluoroethyl derivative [^{18}F]**2** a few trace radiometabolites and two main radiometabolites **2-A** and **2-B** were detected. On the contrary, three major radiometabolites **1-A**, **1-B** and **1-D** in considerably higher amounts were observed for the fluoromethyl derivative [^{18}F]**1**. The number of minor radiometabolites, however, increased at 60 min after injection. In liver samples of mice treated with fluoropropyl and fluorobutyl homologs [^{18}F]**3** and [^{18}F]**4**, several radiometabolites (> 10) were detected by radio-HPLC. Two of these radiometabolites can be considered as major metabolites.

As documented in Table SI1 the recovery of activity after extraction of liver homogenates with CH_3CN was generally rather low. In some experiments, other extracting agents were investigated. Precipitating liver samples containing the fluoromethyl radiotracer [^{18}F]**1** with CH_3OH, led to the same amount of unchanged radiotracer [^{18}F]**1** as found with CH_3CN. However, an additional radiometabolite **1-C** at a retention time of 24.1 min was detected after extraction with CH_3OH, which was not visible after extraction with CH_3CN (Figure 10).

For the fluoroethyl radiotracer [^{18}F]**2**, extraction with more polar solvents such as CH_3OH, aqueous CH_3OH (90% CH_3OH_{aq})

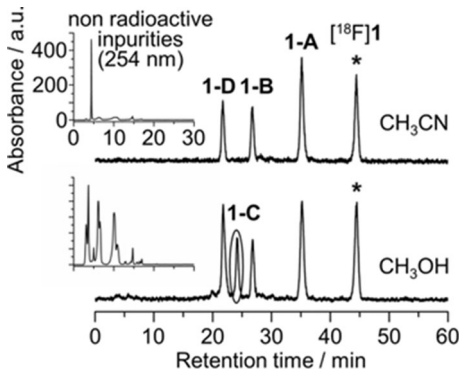

Figure 10. Radiochromatograms of mouse liver samples using different extracting agents. Top: Precipitation with CH_3CN; bottom: Precipitation with CH_3OH; insets: chromatograms with UV detection (254 nm). Liver homogenates were obtained at 30 min after injection of the radiotracer [^{18}F]**1**; the additional radiometabolite is marked in the second chromatogram; retention times of parent compound [^{18}F]**1** and its radiometabolites: [^{18}F]**1**: t_R = 44.5 min; **1-A**: t_R ~ 35 min; **1-B**: t_R ~ 27 min; **1-C**: t_R ~ 24.1 min (additional radiometabolite); **1-D**: t_R ~ 22 min.

or aqueous Ch_3CN (90% CH_3CN_{aq}) resulted in lower recovery of activity than extraction with CH_3CN. However, two very polar radiometabolites with very short retention times (t_R < 4 min) were found after precipitation with aqueous CH_3CN and aqueous CH_3OH. Extraction of liver samples containing the higher homologous fluorobutyl radiotracer [^{18}F]**4** with CH_3OH led to ~10% higher amounts of activity.

Radiometabolites of [^{18}F]1–4 found in mouse plasma

At 30 min after injection, more than 84% of the activity of plasma samples was represented by the unchanged radiotracers [^{18}F]**2**–**4**. Only for the fluoromethyl derivative [^{18}F]**1** was a decreased amount (75%) of intact radiotracer detected. Treatment of the mice for 60 min led to reduced amounts of unchanged radiotracers in the plasma, which can be attributed to increased amounts of radioactive metabolites in the plasma.

In the radio-HPLC chromatograms displayed in Figure 11 (30 min samples) only two small peaks were observed in addition to the unchanged fluorobutyl derivative [^{18}F]**4** (parent radiotracer 84%). These peaks appear at retention times of

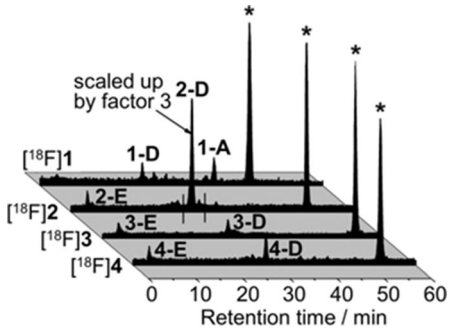

Figure 11. Radiochromatograms of plasma samples 30 min after injection of the radiotracers [^{18}F]**1**–**4** (extraction agent CH_3CN). The peaks of the parent radiotracers are marked with *. The peak for radiometabolite **2-B** of tracer [^{18}F]**2** is increased by a factor of 3.

© 2016 Wiley-VCH Verlag GmbH & Co. KGaA, Weinheim

27.1 min (**4-D**, 14.3%) and 3.5 min (**4-E**, 3.6%). A few further metabolites were detected in traces. A very similar radiochromatogram was obtained for the fluoropropyl derivative [^{18}F]**3** (86% parent) showing two major metabolites at retention times of 25.6 min (**3-D**, 10.3%) and 3.5 min (**3-E**, 3.8%). For the smallest homolog, the fluoromethyl derivative [^{18}F]**1**, several small and two main radioactive metabolites were detected, which correlate nicely with the metabolites **1-A** (37.1 min, 9.5%) and **1-D** (21.7 min, 12.0%) found in tissue samples (only **1-A**). The plasma sample of the fluoroethyl derivative [^{18}F]**2** (89% parent) however reveals a large peak for the radiometabolite **2-D** at a retention time of 28.2 min (5.6%) and a smaller peak at 3.5 min (**2-E**, 5.4%). The formation of the metabolite **2-D** is the reason for decreased amounts of unchanged radiotracer in plasma (Table 2).

Table 2. Amount of recovered parent compounds [^{18}F]**1**–**4** and recovery in mouse plasma 30 min and 60 min after injection (extraction agent: CH_3CN).

Compd	30 min[a]		60 min[a]	
	intact radiotracer [%][b]	recovery [%][c]	intact radiotracer [%][b]	recovery [%][c]
[^{18}F]**1**	75 ± 10	76–80	52 ± 7	60–65
[^{18}F]**2**	89 ± 3	60–75	75 ± 8	50–60
[^{18}F]**3**	86 ± 2	55–65	83 ± 5	60–68
[^{18}F]**4**	84 ± 9	60–70	86 ± 5	67–75

[a] Time after radiotracer injection. [b] Data are mean values ± SD (n = 3–5) from radio-TLC and radio-HPLC experiments. [c] Amount of activity in the CH_3CN extract relative to the total activity in the respective plasma sample.

Figure 12 shows the amount of activity in CH_3CN extracts of mouse plasma related to the injected dose obtained during organ distribution studies.[30,33,36,38] The following trend was observed for plasma samples obtained at 30 min: [^{18}F]**3** > [^{18}F]**4** > [^{18}F]**1** ~ [^{18}F]**2**. The most lipophilic fluorobutyl derivative [^{18}F]**4** revealed the smallest difference between the amount of activity recorded at 30 min and at 60 min as both values are almost identical. On the contrary, the activity amount determined for the more polar radiotracers [^{18}F]**1**–**3** 60 min after injection was decreased to ~50% of the activity obtained at 30 min. Clearly the more polar radiotracers [^{18}F]**1**–**3** are distributed faster into tissues and organs, whereas the more lipophilic fluorobutyl radiotracer [^{18}F]**4** remains in the plasma for a longer time, which could be due to higher plasma protein binding.

Metabolites of [^{18}F]1–4 found in mouse urine

Since urine samples were only available in some experiments, the analysis of radiometabolites was not as exhaustive as for tissue and plasma samples. In Table SI2 the amounts of unchanged radiotracers in urine samples at 30 min and at 60 min after injection of [^{18}F]**1**–**4** is summarized. In the urine samples, only a small amount (< 4%) of parent radiotracers was found. Clearly, the intact radiotracers were not eliminated via the kidney and urine.

On the contrary, up to 10 radiometabolites were detected by analytical HPLC. The majority of radiometabolites were found in trace amounts only, but a few radiometabolites occurred in large amounts (Figure 13, Table 3). For all tracers [^{18}F]**1**–**4**, rather polar radiometabolites **1-E** to **4-E** with a retention time of 3.5 min were detected, which represent major metabolites, in the case of fluoroethyl and fluorobutyl derivatives [^{18}F]**2** and [^{18}F]**4**. The metabolites **1-E** to **4-E** appeared directly after the exclusion volume of the radio-HPLC. It is possible that this peak is caused by [^{18}F]fluoride. However, separate analyses of femur, that is, activity in bone versus marrow, did not indicate any defluorination of the tracers [^{18}F]**1**–**4**. The short retention time in the HPLC analysis indicates the presence of [^{18}F]fluoroethanol or [^{18}F]fluoroacetic acid.

The main metabolites for the four homologous fluoroalkyl derivatives [^{18}F]**1**–**4** are the metabolites **1-C** to **4-C** with retention times of 22–29 min. The increasing retention times from **1-C** to **4-C** are due to increasing chain length. Interestingly, the radiometabolite pattern in the urine of mice treated with [^{18}F]**1** differs considerably from the pattern of the homologous tracers [^{18}F]**2**–**4**. Although the urine is already a solution of the radiometabolites, extraction of the solution with CH_3CN and subsequent analysis of activity led to a recovery of 81% for [^{18}F]**1**, 66% for [^{18}F]**2**, 59% for [^{18}F]**3** and 60% for [^{18}F]**4**.

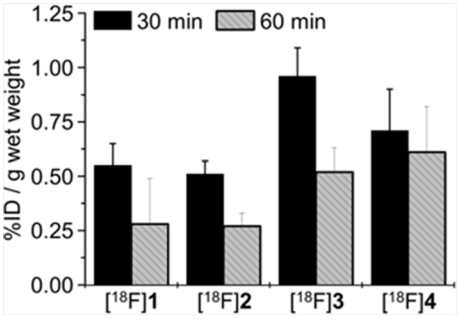

Figure 12. Amount of activity in mouse plasma in relation to the injected dose at 30 min and at 60 min after injection of the radiotracers [^{18}F]**1**–**4**; wet weight normalized dose; data are mean values ± standard deviation, n = 3–5.

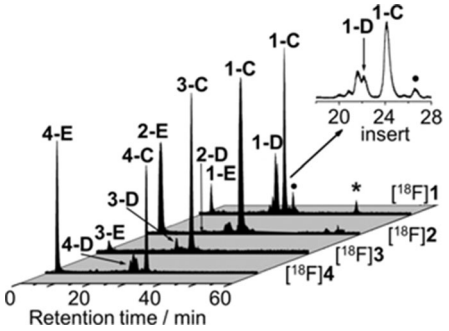

Figure 13. Radiochromatograms of urine samples 30 min after injection of the radiotracers [^{18}F]**1**–**4** (extraction agent CH_3CN). The peaks of the parent radiotracers are marked with *.

© 2016 Wiley-VCH Verlag GmbH & Co. KGaA, Weinheim

Table 3. Relative amounts of major radiometabolites 60 min after injection.[a]

Compd	Metab.	t_R [min]	Amount [%]	Metab.	t_R [min]	Amount [%]	Metab.	t_R [min]	Amount [%]
[^{18}F]**1**	**1-E**	3.5	2–9	**1-D**	22.6	14–29	**1-C**	24.2	47–64
[^{18}F]**2**	**2-E**	3.5	31–48	**2-D**	24.1	5–7	**2-C**	26.3	42–59
[^{18}F]**3**	**3-E**	3.5	4–6	**3-D**	24.3	6–10	**3-C**	26.9	74–89
[^{18}F]**4**	**4-E**	3.6	41–61	**4-D**	24.3	0.10	**4-C**	28.6	23–34

[a] Values are the mean ($n = 2$) from radio-TLC and radio-HPLC experiments.

Comparison of metabolite spectra from brain, liver, plasma and urine using [^{18}F]2 as example

After analyzing the organ-specific radiometabolites separately, the radiometabolite spectra of the homologous tracers [^{18}F]**1**–**4** were compared. Here the fluoroethyl derivative [^{18}F]**2** is discussed. In Figure 14, the radiochromatograms recorded from tissue samples and body fluids at 30 min after application of [^{18}F]**2** are displayed. In the chromatogram of brain samples, only one peak for the unchanged parent compound [^{18}F]**2** is shown indicating that radiometabolites are not formed in the brain and radiometabolites are not able to pass the BBB. In contrast, the urine sample does not contain the parent compound [^{18}F]**2**, but two major very polar radiometabolites **2-D** and **2-E** with retention times of 26.4 min and 3.5 min, respectively. Due to their high polarity these radiometabolites are eliminated via kidney and urine. In the liver and plasma samples the parent compound [^{18}F]**2** represents the major component indicating high metabolic stability. In both samples only trace amounts of the radiometabolites **2-A** ($t_R = 38.2$ min) and **2-B** ($t_R = 31.0$ min) were detected.

The highly polar radiometabolite **2-E** was present predominantly in urine and in low amounts in plasma. Its structure has not yet been identified, but the fast renal elimination inhibits the penetration into various tissues and in particular the CNS.

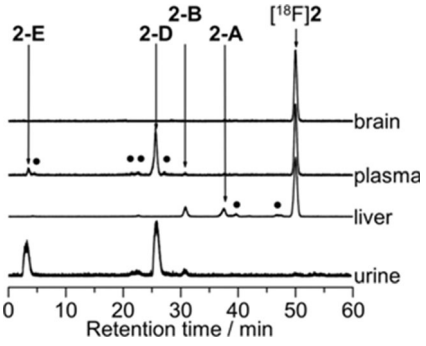

Figure 14. Comparison of radio HPLC chromatograms of samples obtained from different tissues and biofluids at 30 min after injection of the fluoroethyl derivative [^{18}F]**2** (extraction agent CH_3CN); major metabolites are marked with **2-A**, **2-B**, **2-D** and **2-E**; minor metabolites are marked with ●.

Proposed structures of radiometabolites

In order to speculate about the nature of the in vivo formed radiometabolites, the information gained in in vitro studies with rat liver microsomes, electrochemical oxidations and in vivo studies with mice were correlated. The most lipophilic metabolites formed as major metabolites with rat liver microsomes are the hydroxybenzyl derivatives **1c**–**4c**. In vivo, radiometabolites **1-A** to **4-A** represent the most lipophilic radiometabolites, which are also formed as major radiometabolites (see Figure 10–12). Therefore, it can be speculated that the radiometabolites **1-A** to **4-A** formed in vivo bear a hydroxy moiety in the benzyl ring as shown for metabolites **1c**–**4c**.

Debenzylation of the tertiary amines (**1a**–**4a**) represents the second important metabolic pathway catalyzed by CYP enzymes of rat liver microsomes and NADPH. The secondary amines **1a**–**4a** were also detected as major products after electrochemical oxidation and predicted by FAME. As the secondary amines **1a**–**4a** are considerably more polar than metabolites bearing a hydroxy moiety in the phenyl ring (**1c**–**4c**) or in the fluoroalkyl side chain (**1b**–**4b**), we speculate that the radiometabolites **1-D** to **4-D** are the secondary amines [^{18}F]**1a**–**4a**. According to this hypothesis, the less polar radiometabolites marked with **1-B** to **4-B** could bear the hydroxy moiety in the fluoroalkyl side chain corresponding to metabolites **1b**–**4b**.

Conclusions

Different levels of animal experiments provided complementary information about the biotransformation of homologous fluoroalkyl substituted σ_1 receptor ligands **1**–**4**. Theoretical analysis of metabolites using databases (e.g., FAME) does not require any lab experiments. Electrochemical oxidation can be performed without any animal material and provides valuable ideas about oxidatively labile positions in the σ_1 ligands. Although structural information can be derived from these experiments and computational studies, the biological relevance remains to be elucidated. In vitro metabolism studies using rat liver microsomes require liver from rats as native biological material. The degradation rate and the structure of metabolites formed by oxidation with CYP enzymes can be analyzed with this artificial system. However, studies with mice resemble best the fate of a PET tracer in a living organism. Disadvantages of in vivo studies are the requirement of animals and the missing structural information about radiometabolites due to the very low amount of PET tracers used in animal experiments. These drawbacks are compensated by in vitro studies with liver microsomes and electrochemical oxidation.

For in vivo studies, receptor affinity and selectivity as well as radiochemical availability represent important features of PET tracers. However, pharmacokinetic parameters, such as log$D_{7.4}$ value determining the passage of membranes, penetration

© 2016 Wiley-VCH Verlag GmbH & Co. KGaA, Weinheim

into the CNS and biotransformation are also important properties of PET tracers. This study showed that the database (FAME), electrochemical oxidation experiments, in vitro biotransformation with rat liver microsomes and in vivo metabolism studies with mice provided complementary information supporting the final decision, which compound of this series of homologous fluoroalkyl derivatives should be further developed.

In the case of the fluoroalkyl substituted σ_1 ligands [^{18}F]**1**–[^{18}F]**4**, the fluoroethyl and fluoropropyl derivatives [^{18}F]**2** and [^{18}F]**3** revealed a good brain uptake, while their metabolites could not be detected in the brain. Clearly, the radiometabolites detected in liver, plasma and urine are not able to pass the BBB. Considering the high amount in the brain (4.6% of injected dose), the high σ_1 affinity (K_i = 0.59 nM) and the low log$D_{7.4}$ value (2.57), [^{18}F]**2** is the favored radioligand to be further developed as PET tracer.

Experimental Section

In silico prediction of metabolically labile positions

ChemDraw was used to draw the basic amines **1**–**4** as protonated species as they exist at pH 7.4. Then, sdf files were created. These files were used by FAME for the prediction of metabolically labile positions. The applied algorithm included phase 1 reactions from rats ("ratPhase1").

Electrochemical oxidation of 1–4

Compounds **1**–**4**[30,32,36,38] were dissolved in ammonium formate (50/50 (*v/v*) 10 mM, pH 7.4, adjusted with aqueous ammonia) and CH_3CN to a final concentration of 10 μM. The solutions were continuously pumped through an amperometric electrochemical thin-layer cell (ReactorCell, Antec Leyden, Netherlands) equipped with a boron-doped diamond working electrode, a graphite-doped Teflon counter electrode and a Pd/H_2 reference electrode, to which all potentials mentioned in this work refer. The flow rate was set to 10 μL min^{-1}, and a potential ramp between 0 and 2.5 V with a scan rate of 10 mV s^{-1} was applied. The effluent of the electrochemical cell was directly analyzed by means of ESI-HRMS using an Orbitrap mass analyzer (Exactive, Thermo Fisher Scientific, Bremen, Germany). Mass spectra were recorded in the positive ionization mode with the following MS parameters: ESI(+); resolution, high; AGC target, balanced; sheath gas flow (N_2), 10 au; capillary temperature, 275 °C; spray voltage, 4.0 kV; capillary voltage, 95 V; tube lens voltage, 120 V; skimmer voltage, 38 V; maximum injection time, 100 ms; *m/z* range, 100–1000.

In vitro metabolism using rat liver microsomes

Preparation of rat liver microsomes: Frozen rat livers from Wistar rats were thawed in phosphate buffer (pH 7.4) with sucrose (0.25 M) and EDTA (5 mM), cut into pieces and homogenized with a Potter (Elvehjem Potter, B. Braun Biotech International, Melsungen, Germany) at 4 °C. The resulting suspension was centrifuged (high-speed cooling centrifuge model Sorvall, RC-5C plus, Thermo Finnigan, Langerwehe, Germany) at 10000 *g* for 15 min at 4 °C. Fat was removed by absorption with cellulose. The pellet was resuspended in buffer, the mixture centrifuged again and afterward both supernatants were combined. This suspension was transferred into an ultracentrifuge (Beckmann L8M with rotor Ti 70.1) and centrifuged for 60 min at 100000 *g* and 4 °C. The resulting supernatant (cytosol) was discarded, the pellet carefully washed with buffer, resuspended and the centrifugation repeated. Finally the supernatant was removed, the pellet resuspended in a small amount of phosphate buffer (pH 7.4) and the microsome suspension was stored at −80 °C. The protein concentration was determined according to the method of Bradford[48] using bovine serum albumin as standard.

Incubation of 1–4 with rat liver microsomes: The incubation was carried out in phosphate buffer (pH 7.4) at room temperature in a circular shaker (IKA vibrax VXR, Staufen, Germany) and contained rat liver microsomes (1.5 mg mL^{-1} protein), $MgCl_2$ (0.86 mm) and NADPH (2.6 mm). The concentration of **1**–**4** was 260 μM in a final volume of 0.9 mL. Usually, the incubation was stopped after 90 min by addition of cold acetonitrile (−20 °C). The samples were stored for 10 min on ice to complete protein precipitation. After thawing, the samples were centrifuged for 8 min (10000 *g* in Hettich Mikro 20 benchtop centrifuge). The supernatant was decanted, filtered with a 0.45 μm pore size syringe filter made from regenerated cellulose and analyzed.

Structure elucidation by HPLC–MS: The LC–MS system consisted of a LTQ Orbitrap® XL with Accela® HPLC pump and autosampler (Thermo Fisher). The prepared incubation solutions (20 μL) were injected onto a LiChrospher® RP Select B column (5 μm, 250× 4.6 mm) with guard column LiChroCART® RP Select B (4×4.0 mm) at a flow rate of 1.0 mL min^{-1}. The mobile phase was composed of (A) 15% CH_3CN in water and (B) 60% CH_3CN in water; both components contained formic acid (0.1%). The following gradient was applied (A%): 0–20 min: gradient from 100% to 0%, 20–23 min: 0%, 23–24 min: gradient from 0% to 100%, 24–30 min: 100%. For MS analysis the eluent was reduced to 25% by a post-column splitter (Acurate, LC Packings, Dionex). The MS parameters were as follows: ion spray voltage: 4 kV in positive mode, sheath gas flow: 40 arbitrary units, aux gas flow: 15 arbitrary units, sweep gas flow: 10 arbitrary units, capillary temperature: 275 °C, capillary: voltage 40.5 V. First a total ion current (TIC) spectrum was recorded. In order to elucidate the structures of the metabolites, collision induced dissociation (CID), fragmentation experiments were carried out. The Orbitrap MS system generated data with fragmentations up to MS^3.

Metabolic stability: Six incubations of the compounds were carried out in phosphate buffer (pH 7.4) at room temperature in a circular shaker containing rat liver microsomes (1.5 mg mL^{-1} protein), $MgCl_2$ (0.86 mm) and NADPH (2.6 mm). The concentration of compounds **1**–**4** was 320 μM in a final volume of 900 μL. After periods of 5, 10, 30, 40, 60 and 90 min, the incubations were stopped by addition of cold CH_3CN (500 μL, −20 °C). Then praziquantel solution (200 μL, 0.6 mg mL^{-1} in CH_3CN) was added as internal standard resulting in a total volume of 1.6 mL. All incubations were carried out as duplicates. The samples were kept at −20 °C for 30 min to complete protein precipitation. After thawing, the samples were centrifuged at 10000 *g* for 10 min, then the supernatant was decanted, filtered with a 0.45 μm pore size syringe filter made from regenerated cellulose (Macherey–Nagel, Düren, Germany) and analyzed. A calibration was carried out with the same microsomal matrix except NADPH. All calibration standards were treated in the same way (90 min on the shaker, protein precipitation with acetonitrile, centrifugation, etc.). The HPLC analysis was carried out with a Merck Hitachi equipment consisting of UV detector: L-7400; autosampler: L-7200; pump: L-7150; interface: D-7000. Twenty microliters of the prepared incubation solutions were injected onto

© 2016 Wiley-VCH Verlag GmbH & Co. KGaA, Weinheim

a Phenomenex Gemini® C_{18} column (5 μm, 250×4.6 mm) at a flow rate of 1.0 mL min^{-1} and UV detection wavelength of 210 nm. The mobile phase was composed of (A) 15% CH_3CN in water and (B) 60% CH_3CN in water. Trifluoroacetic acid (0.05%) was added to both components. The following gradient was applied (A%): 0–20 min: gradient from 100% to 0%, 20–23 min: 0%, 23–24 min: gradient from 0% to 100%, 24–30 min: 100%.

Data of the metabolites: Exact masses of metabolites and corresponding fragments were determined using LTQ Orbitrap® XL. The exact masses confirm the elemental composition of the postulated metabolites.

Fragmentation of the metabolites of the fluoromethyl derivative 1

Metabolite **1a**: HPLC: t_R=8.3 min. MS^1 (ESI+ exact mass): *m/z* calcd for [$C_{13}H_{16}FNO$+H] 222.1294, found 222.1291. MS^2 (ESI+ exact mass): *m/z* calcd for [$C_{12}H_{14}FN$+H] 204.1189, found 204.1183 [*M*−H_2O].

Metabolite **1b**: HPLC: t_R=12.0 min and 12.7 min (diastereomers). MS^1 (ESI+ exact mass): *m/z* calcd for [$C_{20}H_{22}FNO_2$+H] 328.1713, found 328.1711. MS^2 (ESI+ exact mass): *m/z* calcd for [$C_{10}H_9FO_2$+H] 181.0665, found 181.0659 [*M*−$CH_2C_6H_5$−$N(CH_2)_3$].

Metabolite **1c**: HPLC: t_R=13.5 min. MS^1 (ESI+ exact mass): *m/z* calcd for [$C_{20}H_{22}FNO_2$+H] 328.1713, found 328.1711. MS^2 (ESI+ exact mass): *m/z* calcd for [$C_{13}H_{16}FNO$+H] 222.1294, found 222.1290 [*M*−$CH_2C_6H_4OH$].

Metabolite **1e**: HPLC: t_R=6.0 min. MS^1 (ESI+ exact mass): *m/z* calcd for [$C_{13}H_{16}FNO_2$+H] 238.1234, found 238.1238.

Metabolite **1f**: HPLC: t_R=9.4 min and 9.87 min (isomers). MS^1 (ESI+ exact mass): *m/z* calcd for [$C_{20}H_{22}FNO_3$+H] 344.1662, found 344.1658. MS^2 (ESI+ exact mass): *m/z* calcd for [$C_{20}H_{20}FNO_2$+H] 326.1556, found 326.1551 [*M*−H_2O]. MS^3 (ESI+ exact mass): *m/z* calcd for [$C_{13}H_{14}FNO$+H] 220.1138, found 220.1133 [*M*−H_2O−$CH_2C_6H_4OH$].

Fragmentation of the metabolites of the fluoroethyl derivative 2

Metabolite **2a**: HPLC: t_R=11.1 min. MS^1 (ESI+ exact mass): *m/z* calcd for [$C_{14}H_{18}FNO$+H] 236.1451, found 236.1444. MS^2 (ESI+ exact mass): *m/z* calcd for [$C_{14}H_{16}FN$+H] 218.1345, found 218.1338 [*M*−H_2O].

Metabolite **2b**: HPLC: t_R=13.4 min and 15.4 min (diastereomers). MS^1 (ESI+ exact Mass): *m/z* calcd for [$C_{21}H_{24}FNO_2$+H] 342.1869, found 342.1865. MS^2 (ESI+ exact mass): *m/z* calcd for [$C_{11}H_{11}FO_2$+H] 195.0821, found 195.0813 [*M*−$CH_2C_6H_5$−$N(CH_2)_3$].

Metabolite **2c**: HPLC: t_R=16.6 min and 17.0 min (regioisomers). MS^1 (ESI+ exact mass): *m/z* calcd for [$C_{21}H_{24}FNO_2$+H] 342.1869, found 342.1865. MS^2 (ESI+ exact mass): *m/z* calcd for [$C_{14}H_{18}FNO$+H] 236.1451, found 236.1444 [*M*−$CH_2C_6H_4OH$].

Metabolite **2e**: HPLC: t_R=6.6 min. MS^1 (ESI+ exact mass): *m/z* calcd for [$C_{14}H_{18}FNO_2$+H] 252.1400, found 252.1392.

Metabolite **2f**: HPLC: t_R=10.7 min. MS^1 (ESI+ exact mass): *m/z* calcd for [$C_{21}H_{24}FNO_3$+H] 358.1818, found 358.1810. MS^2 (ESI+ exact mass): *m/z* calcd for [$C_{21}H_{22}FNO_2$+H] 340.1713, found 340.1704 [*M*−H_2O]. MS^3 (ESI+ exact mass): *m/z* calcd for [$C_{14}H_{16}FNO$+H] 234.1284, found 234.1284 [*M*−H_2O−$CH_2C_6H_4OH$].

Fragmentation of the metabolites of the fluoropropyl derivative 3

Metabolite **3a**: HPLC: t_R=12.6 min. MS^1 (ESI+ exact mass): *m/z* calcd for [$C_{15}H_{20}FNO$+H] 250.1602, found 250.1602. MS^2 (ESI+ exact mass): *m/z* calcd for [$C_{15}H_{18}FN$+H] 232.1496, found 232.1493 [*M*−H_2O].

Metabolite **3b**: HPLC: t_R=15.1 min and 16.9 min (diastereomers). MS^1 (ESI+ exact mass): *m/z* calcd for [$C_{22}H_{26}FNO_2$+H] 356.2020, found 356.2016. MS^2 (ESI+ exact mass): *m/z* calcd for [$C_{12}H_{13}FO_2$+H] 209.0972, found 209.0969 [*M*−$CH_2C_6H_5$−$N(CH_2)_3$].

Metabolite **3c**: HPLC: t_R=18.3 min and 18.6 min (regioisomers). MS^1 (ESI+ exact mass): *m/z* calcd for [$C_{22}H_{26}FNO_2$+H] 356.2020, found 356.2016. MS^2 (ESI+ exact mass): *m/z* calcd for [$C_{15}H_{20}FNO$+H] 250.1602, found 250.1598 [*M*−$CH_2C_6H_4OH$].

Metabolite **3e**: HPLC: t_R=8.1 min. MS^1 (ESI+ exact mass): *m/z* calcd for [$C_{15}H_{20}FNO_2$+H] 266.1551, found 266.1551.

Metabolite **3f**: HPLC: t_R=12.6 min. MS^1 (ESI+ exact mass): *m/z* calcd for [$C_{22}H_{26}FNO_3$+H] 372.1969, found 372.1969. MS^2 (ESI+ exact mass): *m/z* calcd for [$C_{22}H_{24}FNO_2$+H] 354.1864, found 354.1863 [*M*−H_2O]. MS^3 (ESI+ exact mass): *m/z* calcd for [$C_{15}H_{18}FNO$+H] 248.1445, found 248.1445 [*M*−H_2O−$CH_2C_6H_4OH$].

Fragmentation of the metabolites of the fluorobutyl derivative 4

Metabolite **4a**: HPLC: t_R=14.9 min. MS^1 (ESI+ exact mass): *m/z* calcd for [$C_{16}H_{22}FNO$+H] 264.1764, found 264.1758. MS^2 (ESI+ exact mass): *m/z* calcd for [$C_{16}H_{20}FN$+H] 246.1658, found 246.1654 [*M*−H_2O].

Metabolite **4b**: HPLC: t_R=20.2 min and 20.6 min (diastereomers). MS^1 (ESI+ exact mass): *m/z* calcd for [$C_{23}H_{28}FNO_2$+H] 370.2182, found 370.2176. MS^2 (ESI+ exact mass): *m/z* calcd for [$C_{12}H_{13}FO_2$+H] 223.1134, found 223.1129 [*M*−$CH_2C_6H_5$−$N(CH_2)_3$].

Metabolite **4c**: HPLC: t_R=14.6 min and 18.8 min (regioisomers). MS^1 (ESI+ exact mass): *m/z* calcd for [$C_{23}H_{28}FNO_2$+H] 370.2182, found 370.2176. MS^2 (ESI+ exact mass): *m/z* calcd for [$C_{15}H_{20}FNO$+H] 264.1764, found 264.1758 [*M*−$CH_2C_6H_4OH$].

Metabolite **4e**: HPLC: t_R=9.8 min. MS^1 (ESI+ exact mass): *m/z* calcd for [$C_{16}H_{22}FNO_2$+H] 280.1713, found 280.1709.

Metabolite **4f**: HPLC: t_R=14.5 min. MS^1 (ESI+ exact mass): *m/z* calcd for [$C_{23}H_{28}FNO_3$+H] 386.2131, found 386.2128 MS^2 (ESI+ exact mass): *m/z* calcd for [$C_{23}H_{26}FNO_2$+H] 368.2026, found 368.2023 [*M*−H_2O]. MS^3 (ESI+ exact mass): *m/z* calcd for [$C_{16}H_{20}FNO$+H] 262.1607, found 262.1604 [*M*−H_2O−$CH_2C_6H_4OH$].

In vivo metabolism of radiofluorinated σ_1 ligands [^{18}F]1–4 in mice

Animal experiments: All procedures involving animals were carried out according to the Principles of Laboratory Animal Care (NIH publication No. 86-23, revised 1985) and following the national laws on the protection of animals. For the HZDR group, the studies were performed based on an authorized approval (Landesdirektion Leipzig, No. 24-9168, 11/12/23; TVV 22/10).

Radiosynthesis: Aqueous [^{18}F]fluoride solution was transformed into the reactive K[^{18}F]F–K2.2.2–carbonate complex using K_2CO_3 (1.8 mg, 12.9 μmol) and K2.2.2 (Kryptofix, 11.2 mg, 29.7 μmol). This

© 2016 Wiley-VCH Verlag GmbH & Co. KGaA, Weinheim

complex was reacted with tosylates **5**–**8** (2.5–3 mg) dissolved in anhydrous CH_3CN (1 mL). The mixture was heated at 85 °C for 15 min. For the synthesis of [^{18}F]**1** the transformation was performed in DMSO (1 mL) and the mixture was heated at 150 °C for 25 min. The resulting mixture was diluted with water (3 mL) and directly applied to an isocratic semi-preparative HPLC for purification (Multispher® 120 RP18 AQ column, 150×10 mm, particle size 5 μm with guard column, 50×10 mm, 5 μm); eluent: CH_3CN (55%) with NH_4OAc (20 mm), flow rate 4.0 mL min^{-1}. The fractions containing the respective radiotracer were combined, diluted with water, passed through a pre-conditioned Sep-Pak C_{18} cartridge, and the purified radiotracer was eluted with CH_3OH (~1.5 mL). For in vivo experiments, the solvent was evaporated and the radiotracer was re-dissolved in saline.

Radio-thin-layer chromatography (radio-TLC):

Radio-thin-layer chromatography (radio-TLC) was performed using SIL G/UV_{254} precoated plates using different mixtures of ethyl acetate/petroleum ether/NH_3; (*v*/*v*/*v*) as optimized standard procedure. All data are based on duplicate values. Spots were visualized under UV light (254 nm) and by radioluminescence recording (BAS-1800 II Bioimaging Analyzer, Fuji film, Tokyo, Japan), and quantitatively evaluated with AIDA 2.31 software (raytest, Straubenhardt, Germany). Alternative eluents were applied: ethyl acetate/CH_3OH varying between 95:5 to 80:20 (*v*/*v*) and CH_2Cl_2/CH_3OH/NEt_3 = 8:2:0.1. R_f values of the reference compounds of the corresponding radiotracers: **1**: R_f = 0.74 (ethyl acetate/petroleum ether/NH_3 5:5:0.1); **2**: R_f = 0.54 (ethyl acetate/petroleum ether/NH_3 3:7:0.1); **3**: R_f = 0.61 (ethyl acetate/petroleum ether/NH_3 3:7:0.1); **4**: R_f = 0.52 (ethyl acetate/petroleum ether/NH_3 3:7:0.1).

Radio-HPLC

Method 1: Agilent device (HPLC 1100 ChemStation; quaternary pump, degasser, multiwavelength detector), coupled with a radioactivity-HPLC flow monitor (FAP 100k/HV, bte, Germany); Multospher 120 RP18 AQ 250×4.6 mm, 5 μm with guard column (10×4.6 mm, 5 μm) (CS Chromatographie Service, Germany); gradient: 5–80% CH_3CN/20 mmol NH_4OAc; 1.0 mL min^{-1}; run time: ~60–70 min; solution A: 5% CH_3CN + 20 mm NH_4OAc; solution B: 80% CH_3CN + 20 mm NH_4OAc; gradient: 0–10 min (100% A) 10–50 min (solution B increasing from 0% to 100%), 50–60 min. In few cases an isocratic method using 42.5% CH_3CN + 20 mm NH_4OAc as mobile phase was used.

Method 2: Jasco HPLC Serie 2000 (interface LC-NET II ADC; pumps: binary p., quaternary HP gradient system p.; 4-line-degassers; autosampler; UV/Vis detectors; coupled with radioactivity-HPLC-low-monitors (Gabi Star, raytest GmbH, Germany), software Chrompass; Reprosil-Pur C_{18}-AQ 250×4.6 mm, 5 μm with guard column (Dr. Maisch GmbH, Ammerbuch-Entringen, Germany); gradient 10–90% CH_3CN/20 mm NH_4OAc.

Preparation of tissue samples: For the investigation of radiometabolites, radiotracers [^{18}F]**1**–[^{18}F]**4** (~200–300 MBq) were administered to female CD-1 mice by tail vein injection. After 30 or 60 min, brain and liver samples were homogenized and plasma and urine were directly used. Mouse brain or liver was homogenized with the Potter (500–800 rpm, 10 up-and-down strokes) in six volumes of cold sucrose (0.3 m). The suspension was centrifuged at 1000 *g* for 10 min at 4 °C. The supernatant was separated and centrifuged at 23 500 *g* for 20 min at 4 °C. The pellet was resuspended in 5–6 volumes of buffer (500 mm Tris buffer, pH 7.4) and centrifuged again at 23 500 *g* for 20 min at 4 °C. This procedure was repeated twice. The final pellet was resuspended in 5–6 volumes of buffer. The precipitation of proteins in brain, liver, plasma and urine samples was performed by addition of four volumes of ice-cold acetonitrile. The precipitate was removed by centrifugation and the supernatant was concentrated (60 °C, air flow).

Recovery of PET tracer [^{18}F]2 from complex biological matrices: Plastic tubes were filled with extracting agent (500 μL). Then, the biological sample was added in a ratio of about 4:1 to 7:1 (extracting agent/biological sample). The samples were vortexed and kept in an ice bath for 15 min. After centrifugation, the supernatants of all aliquots were combined and concentrated with argon gas and gentle warming (~60 °C) up to a final residual volume of ~150 μL. The activity of the extract was recorded and related to the activity of the biological sample. Recovery (%) in this article is defined as the activity of the extract divided by the activity of the original biological sample multiplied by 100%. The percentages of parent radiotracer and radiometabolites were analyzed by radio-HPLC and radio-TLC. Data obtained for all radiotracers are based on repetitive analyses (n = 2–5). In general, good agreement was achieved between radio-HPLC and radio-TLC data (deviations for brain and urine ~1%, for plasma ≤5–8% and liver ≤5%). Here, both inter-individual variability of mice, methodical discrepancies and the analytical error have to be considered.

In general acetonitrile was used as standard precipitating and extracting agent. In experiments regarding the recovery of activity, additional precipitating agents such as pure methanol, aqueous methanol (90% CH_3OH_{aq}) and aqueous acetonitrile (90% CH_3CN_{aq}) were investigated.

For comparative metabolite studies, non-native biological samples preserved as Tris buffer solutions and stored in a deep freezer or obtained from fresh ex vivo samples were applied. They included plasma (rabbit), brain homogenate (mouse), and liver (pig). For this purpose, tissue material (50–75 μL) or biofluids was mixed with radiotracer in saline (~10 μL, ~1–5 MBq) and extractive agent (500 μL) and processed as described before for in vivo metabolite experiments.

γ-counting: The extraction efficiency of the total ^{18}F activity ("activity balance" recovery) was monitored permanently for each step and aliquots were measured by gamma counting of the supernatants and precipitates using a calibrated gamma counter (Wallac WIZARD 3, PerkinElmer, USA).

Protein determination according to the method of Bradford: The amount of residual proteins in supernatants was determined by photometric analysis with the BCA method[48] using a bovine serum albumin standard (PerkinElmer) and a microplate reader (BIORAD Model 680 microplate reader, Bio-Rad Laboratories, Germany); Windows based Microplate Manager software; 96-well microtiter plate; Instruction Thermo Scientific Pierce BCA Protein Assay Kit [23225/23227] (Pierce Biotechnology, Rockford, USA).

Author contributions

C.W., D.S., P.B., U.K., and B.W. participated in the research design; C.W., E.G.M., A.H., S.F., F.A.L., W.D.-C., C.D., and L.B. contributed experiments; F.G. contributed to the reagents or analytical tools; F.G. and C.D. performed data analysis; A.H., S.F., U.K., and B.W. wrote or contributed to the writing of the manuscript. The authors declare no conflicts of interest.

© 2016 Wiley-VCH Verlag GmbH & Co. KGaA, Weinheim

Acknowledgements

This work was performed within the framework of the International Research Training Group (IRTG) 'Complex Functional Systems in Chemistry: Design, Synthesis and Applications' in collaboration with Nagoya University. Financial support of the IRTG and this project by the Deutsche Forschungsgemeinschaft (DFG) is gratefully acknowledged. The authors thank Prof. Dr. J. Kirchmair for providing the FAME software.

Keywords: biotransformation · electrochemistry · fluorination · metabolism · oxidation · positron emission tomography · σ_1 receptor ligands

[1] G. P. Martin, C. Marriott, I. W. Kellaway, *J. Pharm. Pharmacol.* **1976**, *28*, 76P.
[2] T. P. Su, *J. Pharmacol. Exp. Ther.* **1982**, *223*, 284 – 290.
[3] D. B. Vaupel, *Eur. J. Pharmacol.* **1983**, *92*, 269 – 274.
[4] R. Quirion, W. D. Bowen, Y. Itzhak, L. Junien, J. M. Musacchio, R. B. Rothman, T. P. Su, S. W. Tam, D. P. Taylor, *Trends Pharmacol. Sci.* **1992**, *13*, 85 – 86.
[5] S. B. Hellewell, A. Bruce, G. Feinstein, J. Orringer, W. Williams, W. D. Bowen, *Eur. J. Pharmacol.* **1994**, *268*, 9 – 18.
[6] R. Kekuda, P. D. Prasad, Y. J. Fei, F. H. Leibach, V. Ganapathy, *Biochem. Biophys. Res. Commun.* **1996**, *229*, 553 – 558.
[7] F. F. Moebius, R. J. Reiter, M. Hanner, H. Glossmann, *Br. J. Pharmacol.* **1997**, *121*, 1 – 6.
[8] S. Brune, S. Pricl, B. Wünsch, *J. Med. Chem.* **2013**, *56*, 9809 – 9819.
[9] E. Laurini, V. Dal Col, M. G. Mamolo, D. Zampieri, P. Posocco, M. Fermeglia, V. Vio, S. Pricl, *ACS Med. Chem. Lett.* **2011**, *2*, 834 – 839.
[10] S. Brune, D. Schepmann, K.-H. Klempnauer, D. Marson, V. Dal Col, E. Laurini, M. Fermeglia, B. Wünsch, S. Pricl, *Biochemistry* **2014**, *53*, 2993 – 3003.
[11] T. Hayashi, S. Y. Tsai, T. Mori, M. Fujimoto, T. P. Su, *Expert Opin. Ther. Targets* **2011**, *15*, 557 – 577.
[12] T. Hayashi, T. P. Su, *Cell* **2007**, *131*, 596 – 610.
[13] T. P. Su, T. Hayashi, T. Maurice, S. Buch, A. E. Ruoho, *Trends Pharmacol. Sci.* **2010**, *31*, 557 – 566.
[14] P. D. Lupardus, R. A. Wilke, E. Aydar, C. P. Palmer, Y. Chen, A. E. Ruoho, M. B. Jackson, *J. Physiol.* **2000**, *526*, 527 – 539.
[15] M. Johannessen, S. Ramachandran, L. Riemer, A. Ramos-Serrano, A. E. Ruoho, M. B. Jackson, *Am. J. Physiol. Cell Physiol.* **2009**, *296*, C1049 – C1057.
[16] T. Maurice, T. P. Su, *Pharmacol. Ther.* **2009**, *124*, 195 – 206.
[17] G. Navarro, E. Moreno, M. Aymerich, D. Marcellino, P. J. McCormick, J. Mallol, A. Cortes, V. Casado, E. I. Canela, J. Ortiz, K. Fuxe, C. Lluis, S. Ferre, R. Franco, *Proc. Natl. Acad. Sci. USA* **2010**, *107*, 18676 – 18681.
[18] S. J. Nuwayhid, L. L. Werling, *J. Pharmacol. Exp. Ther.* **2003**, *304*, 364 – 369.
[19] C. Ela, J. Barg, Z. Vogel, Y. Hasin, Y. Eilam, *J. Pharmacol. Exp. Ther.* **1994**, *269*, 1300 – 1309.
[20] S. A. Wolfe, Jr., S. G. Culp, E. B. De Souza, *Endocrinology* **1989**, *124*, 1160 – 1172.
[21] S. A. Wolfe, Jr., C. Kulsakdinun, G. Battaglia, J. H. Jaffe, E. B. De Souza, *J. Pharmacol. Exp. Ther.* **1988**, *247*, 1114 – 1119.
[22] E. J. Cobos, J. M. Entrena, F. R. Nieto, C. M. Cendán, E. Del Pozo, *Curr. Neuropharmacol.* **2008**, *6*, 344 – 366.
[23] T. Hayashi, T. P. Su, *CNS Drugs* **2004**, *18*, 269 – 284.
[24] T. Maurice, J. Meunier, B. Feng, J. Ieni, D. T. Monaghan, *J. Pharmacol. Exp. Ther.* **2006**, *317*, 606 – 614.
[25] X. Guitart, X. Codony, X. Monroy, *Psychopharmacology* **2004**, *174*, 301 – 319.
[26] J. L. Diaz, D. Zamanillo, J. Corbera, J. M. Baeyens, R. Maldonado, M. A. Pericas, J. M. Vela, A. Torrens, *Cent. Nerv. Syst. Agents Med. Chem.* **2009**, *9*, 172 – 183.
[27] J. M. Entrena, E. J. Cobos, F. R. Nieto, C. M. Cendan, G. Gris, E. Del Pozo, D. Zamanillo, M. Baeyens, *Pain* **2009**, *143*, 252 – 261.
[28] B. Wünsch, *J. Med. Chem.* **2012**, *55*, 8209 – 8210.
[29] P. Brust, W. Deuther-Conrad, K. Lehmkuhl, H. Jia, B. Wünsch, *Current Med. Chem.* **2014**, *21*, 35 – 69.
[30] A. Maisonial, E. Große Maestrup, C. Wiese, A. Hiller, D. Schepmann, S. Fischer, W. Deuther-Conrad, J. Steinbach, P. Brust, B. Wünsch, *Bioorg. Med. Chem.* **2012**, *20*, 257 – 269.
[31] K. Holl, D. Schepmann, C. G. Daniliuc, B. Wünsch, *Tetrahedron: Asymmetry* **2014**, *25*, 268 – 277.
[32] E. Große Maestrup, C. Wiese, D. Schepmann, P. Brust, B. Wünsch, *Bioorg. Med. Chem.* **2011**, *19*, 393 – 405.
[33] S. Fischer, C. Wiese, E. Große Maestrup, A. Hiller, W. Deuther-Conrad, M. Scheunemann, D. Schepmann, J. Steinbach, B. Wünsch, P. Brust, *Eur. J. Nucl. Med. Mol. Imaging* **2011**, *38*, 540 – 551.
[34] K. Holl, E. Falck, J. Köhler, D. Schepmann, H.-U. Humpf, P. Brust, B. Wünsch, *ChemMedChem* **2013**, *8*, 2047 – 2056.
[35] A. Maisonial-Besset, U. Funke, B. Wenzel, S. Fischer, K. Holl, J. Steinbach, P. Brust, B. Wünsch, *Appl. Radiat. Isot.* **2014**, *84*, 1 – 7.
[36] E. Große Maestrup, S. Fischer, C. Wiese, D. Schepmann, A. Hiller, W. Deuther-Conrad, J. Steinbach, B. Wünsch, P. Brust, *J. Med. Chem.* **2009**, *52*, 6062 – 6072.
[37] C. Wiese, E. Große Maestrup, D. Schepmann, S. Grimme, H.-U. Humpf, P. Brust, B. Wünsch, *Chirality* **2011**, *23*, 148 – 154.
[38] A. Maisonial, E. Große Maestrup, S. Fischer, A. Hiller, M. Scheunemann, C. Wiese, D. Schepmann, J. Steinbach, W. Deuther-Conrad, B. Wünsch, P. Brust, *ChemMedChem* **2011**, *6*, 1401 – 1410.
[39] J. Kirchmair, M. J. Williamson, A. M. Afzal, J. D. Tyzack, A. P. Choy, A. Howlett, P. Rydberg, R. C. Glen, *J. Chem. Inf. Model.* **2013**, *53*, 2896 – 2907.
[40] L. Büter, M. Vogel, U. Karst, *TrAC Trends Anal. Chem.* **2015**, *70*, 74 – 91.
[41] U. Jurva, H. V. Wikström, L. Weidolf, A. P. Bruins, *Rapid Commun. Mass Spectrom.* **2003**, *17*, 800 – 810.
[42] H. Faber, M. Vogel, U. Karst, *Anal. Chim. Acta* **2014**, *834*, 9 – 21.
[43] E. Nouri-Nigjeh, R. Bischoff, A. P. Bruins, H. P. Permentier, *Curr. Drug Metab.* **2011**, *12*, 359 – 371.
[44] F. T. van den Brink, L. Büter, M. Odijk, W. Olthuis, U. Karst, A. van den Berg, *Anal. Chem.* **2015**, *87*, 1527 – 1535.
[45] H. Pham-Tuan, L. Kaskavelis, C. A. Daykin, H.-G. Janssen, *J. Chromatogr. B* **2003**, *789*, 283 – 301.
[46] H. Mascher, *Klinische Analytik mit HPLC: Ein Ratgeber für die Praxis*, Wiley-VCH, Weinheim, **2010**.
[47] M. J. Welch, D. Y. Chi, C. J. Mathias, M. R. Kilbourn, J. W. Brodack, J. A. Katzenellenbogen, *Nucl. Med. Biol.* **1986**, *13*, 523 – 526.
[48] M. M. Bradford, *Anal. Biochem.* **1976**, *72*, 248 – 254.

Received: July 19, 2016
Revised: August 29, 2016
Published online on ■■ ■■, 0000

© 2016 Wiley-VCH Verlag GmbH & Co. KGaA, Weinheim

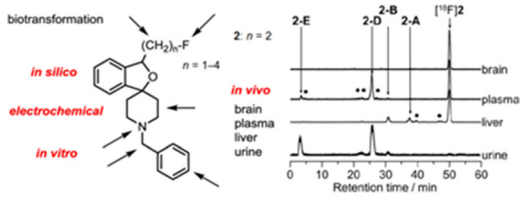

Taking a close look: The biotransformation of a homologous series of fluoroalkyl-substituted σ_1 receptor ligands designed as PET tracers was investigated at different levels: in silico using FAME software, electrochemically, in vitro, and in vivo. Electrochemical oxidation and in vitro studies with rat liver microsomes combined with LC–MS analysis allowed identification of the metabolite structure. The nature and amount of radiometabolites in various tissues were analyzed by radio-HPLC and radio-TLC after application of the [^{18}F]-labeled PET tracers to mice.

*C. Wiese, E. Große Maestrup, F. Galla, D. Schepmann, A. Hiller, S. Fischer, F.-A. Ludwig, W. Deuther-Conrad, C. K. Donat, P. Brust, L. Büter, U. Karst, B. Wünsch**

■■ – ■■

Comparison of in Silico, Electrochemical, in Vitro and in Vivo Metabolism of a Homologous Series of (Radio)fluorinated σ_1 Receptor Ligands Designed for Positron Emission Tomography

© 2016 Wiley-VCH Verlag GmbH & Co. KGaA, Weinheim